Nogo-A targeted therapy promotes vascular repair and functional recovery following stroke

Ruslan Rust[a,b,1], Lisa Grönnert[a], Christina Gantner[c], Alinda Enzler[b], Geertje Mulders[a], Rebecca Z. Weber[a], Arthur Siewert[d], Yanuar D. P. Limasale[e], Andrea Meinhardt[e], Michael A. Maurer[a], Andrea M. Sartori[a,b], Anna-Sophie Hofer[a,b], Carsten Werner[e], and Martin E. Schwab[a,b,1]

[a]Institute for Regenerative Medicine, University of Zurich, 8952 Schlieren, Switzerland; [b]Department of Health Sciences and Technology, ETH Zurich, 8092 Zurich, Switzerland; [c]Department of Biology, ETH Zurich, 8093 Zurich, Switzerland; [d]Department of Technology, Bielefeld University, 33615 Bielefeld, Germany; and [e]Leibniz Institute for Polymer Research, 01069 Dresden, Germany

Edited by Michael E. Greenberg, Harvard Medical School, Boston, MA, and approved May 31, 2019 (received for review March 28, 2019)

Stroke is a major cause of serious disability due to the brain's limited capacity to regenerate damaged tissue and neuronal circuits. After ischemic injury, a multiphasic degenerative and inflammatory response is coupled with severely restricted vascular and neuronal repair, resulting in permanent functional deficits. Although clinical evidence indicates that revascularization of the ischemic brain regions is crucial for functional recovery, no therapeutics that promote angiogenesis after cerebral stroke are currently available. Besides vascular growth factors, guidance molecules have been identified to regulate aspects of angiogenesis in the central nervous system (CNS) and may provide targets for therapeutic angiogenesis. In this study, we demonstrate that genetic deletion of the neurite outgrowth inhibitor Nogo-A or one of its corresponding receptors, S1PR2, improves vascular sprouting and repair and reduces neurological deficits after cerebral ischemia in mice. These findings were reproduced in a therapeutic approach using intrathecal anti–Nogo-A antibodies; such a therapy is currently in clinical testing for spinal cord injury. These results provide a basis for a therapeutic blockage of inhibitory guidance molecules to improve vascular and neural repair after ischemic CNS injuries.

ischemia | therapeutic angiogenesis | revascularization | guidance factor | CNS

A substantial proportion of patients surviving a stroke suffer from mild to severe disabilities due to the brain's limited regenerative capacity (1, 2). Stroke is a major cause of severe disability due to the brain's limited capacity to regenerate damaged tissue. The lack of an effective therapy that promotes long-term recovery after stroke represents a substantial clinical burden and an unmet need for medical treatment outside the confines of conventional thrombolytic and rehabilitative therapies (1). An approach that gained recent interest is the enhancement of vascular repair in the ischemic border zone with the aim to prevent secondary damage and create a permissive microenvironment for tissue recovery and regeneration. Vascular remodeling after stroke has been strongly associated with higher survival rates and improved long-term neurological function in animal models and stroke patients (3–6). To enhance vascular repair, many previous studies have focused on the delivery of proangiogenic growth factors, in particular VEGF, but have been of limited success (7). This was partially due to the fact that VEGF can exacerbate brain damage by promoting blood–brain-barrier (BBB) permeability and the risk for hemorrhages (8).

Besides growth factors, axonal guidance molecules have been recently shown to regulate blood vessel sprouting and migration during development and disease (9–11). Due to similarities in the vascular and nervous innervation pattern, both systems have developed specialized sensory and motile structures: endothelial tip cells (12) and axonal growth cones (13) for sensing, at least in part, similar guidance cues (9, 10). Recently, the neurite outgrowth inhibitor Nogo-A was revealed to also function as an antiangiogenic regulator in brain and retinal development (14, 15); however, its effect on adult or diseased brain vasculature is completely unknown.

Here, we show that interference with Nogo-A signaling after focal cerebral ischemia induces enhanced regrowth of the partially damaged vascular network, which is associated with behavioral improvements. The function-improving effect was lost when the angiogenic response was blocked. Nogo-A genetic deletion, knockout of the Nogo-A receptor component sphingosine 1-phosphate receptor 2 (S1PR2), and the application of anti–Nogo-A antibodies all led to improved vascular repair and thus may represent a therapeutic option for cerebral ischemia.

Results

Vascular Repair Is Limited in the Ischemic Border Zone Despite Up-Regulation of Growth Factors, Resulting in Long-Term Ischemic Conditions. We characterized the expression profiles of a number of marker genes associated with tissue ischemia, vascular growth, and remodeling in the periinfarct region surrounding the core of focal, permanent photothrombotic strokes in adult C57BL/6 mice at days 2, 7, 16, and 28 after injury (Fig. 1*A*). Expression of mRNA extracted from microdissected periinfarct tissue was assessed for genes characteristic for (*i*) sprouting

Significance

Patients suffering from ischemic strokes have limited therapeutic options and are often left with considerable disabilities. To promote neurological recovery, angiogenesis has been proposed as a promising therapeutic target. So far, experimental efforts to enhance vessel growth have almost exclusively focused on vascular growth factor supplementation; this approach has been shown not to be clinically viable due to hemorrhagic risks. Here, we pursued an alternative approach by targeting the guidance molecule Nogo-A, which has been recently shown to inhibit developmental central nervous system angiogenesis. Blockage of the Nogo-A pathway results in restoration of a mature vascular bed within the periinfarct zone. Moreover, we observe enhanced recovery-associated tissue responses and regain of motor functions that strongly correlate with vascular growth.

Author contributions: R.R. and M.E.S. designed research; R.R., L.G., C.G., G.M., R.Z.W., Y.D.P.L., A.M., A.M.S., and A.-S.H. performed research; R.R., Y.D.P.L., A.M., M.A.M., and C.W. contributed new reagents/analytic tools; R.R., L.G., A.E., and A.S. analyzed data; and R.R., L.G., C.W., and M.E.S. wrote the paper.

Conflict of interest statement: M.E.S. is a founder and board member of the University of Zurich spin-off company NovaGo Therapeutics Inc., seeking to develop antibody-based therapies for neurological diseases.

This article is a PNAS Direct Submission.

[1]To whom correspondence may be addressed. Email: rust@irem.uzh.ch or schwab@irem.uzh.ch.

This article contains supporting information online at www.pnas.org/lookup/suppl/doi:10.1073/pnas.1905309116/-/DCSupplemental.

Published online June 24, 2019.

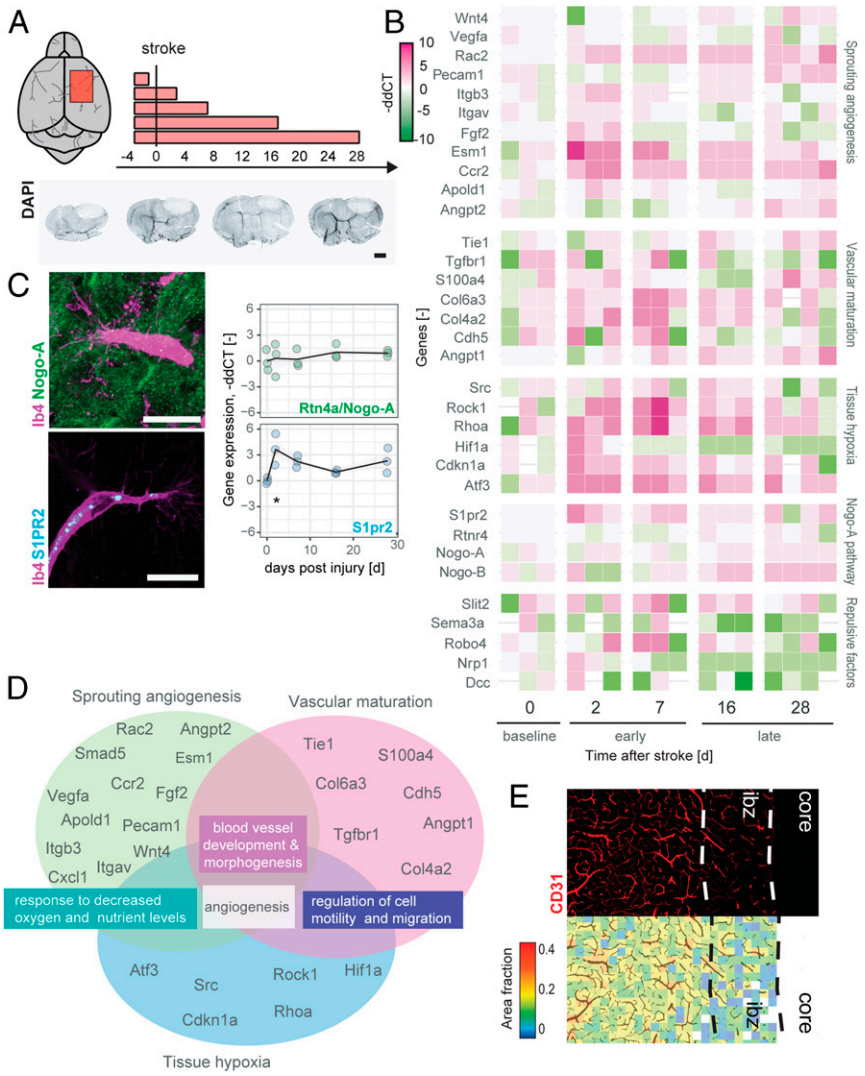

Fig. 1. Angiogenic response after photothrombotic stroke. (*A*) Location of stroke, time points, and histological stroke size. (Scale bar, 1 mm.) (*B*) Expression analysis of genes associated with sprouting angiogenesis, vascular maturation, tissue hypoxia, guidance, and Nogo-A pathway at 2 ($n = 3$), 7 ($n = 3$), 16 ($n = 3$), and 28 ($n = 4$) d postinjury. Data are presented as log expression ratio (-DDCT); purple indicates up-regulation and green indicates down-regulation. (*C*) Representative immunofluorescence images of Nogo-A (*Upper*) and S1PR2 (*Lower*) costained with the vascular endothelium marker Ib4 4 wk after stroke (*Left*) (Scale bars, 20 μm.) Time series of *Rtn4a/Nogo-A* and *S1pr2* expression after stroke in three mice per time point (*Right*). (*D*) Visual representation of the analyzed angiogenesis associated genes according to ontology and function. (*E*) Representative fluorescence image of hypovascularized 300-μm ischemic border zone stained for the vascular marker CD31 4 wk after stroke with corresponding heat maps of local vascular area fraction. Ibz, ischemic border zone. (Scale bar, 100 μm.) Data are mean ± SEM (one-way ANOVA with Dunnett's post hoc test). $^*P < 0.05$.

angiogenesis (ANG), (*ii*) vascular maturation and remodeling (VMR), (*iii*) tissue hypoxia and blood–brain-barrier damage (HYP), and (*iv*) guidance cues. The selection of genes was based on previous observations from transcriptomic data in poststroke angiogenesis (16). We observed a strong, transient up-regulation in a number of genes involved in sprouting angiogenesis (*Esm1*, *Fgf2*, *Itgb3*, and *Rac2*) and vessel formation and maturation (*Col4a2*, *Col6a3*, and *S100a4*) at early time points day 2 (ANG: $P < 0.001$; VMR $P = 0.163$) and partially day 7 (ANG: $P < 0.037$, VMR: $P = 0.239$). Many genes of these clusters were down-regulated back to baseline levels baseline 4 wk after stroke (ANG: $P = 0.450$; VMR: $P = 0.788$). We also found an up-regulation of genes related to hypoxia and blood–brain-barrier damage (*Atf3*, *Cdkn1*, *Rock1*, and *Rhoa*) at day 2 (HYP: $P = 0.075$) and day 7 (HYP: $P = 0.022$) following stroke. Remarkably, most of these genes remained up-regulated, indicating a chronically ischemic and hypovascularized state of this region (Fig. 1 *B* and *D*). These findings were supported by histological evidence of a massive and sustained hypovascularization observed up to 28 d after injury in periinfarct regions (Fig. 1*E*).

Apart from vascular growth- and maturation-promoting genes, we also observed the expression of inhibitory neural and vascular factors in the periinfarct region (9). Several of these ligands or receptors were up-regulated after stroke (*Robo4*, *S1pr2*, *Slit2*, and *Rtn4a/Nogo-A*); some remained elevated up to 4 wk after the injury (*Rtn4a/Nogo-A*, *Rtn4b/Nogo-B*, *Rtnr4*, *Slit2*, and *S1pr2*). Among these, the Nogo-A (Rtn4a) receptor, S1PR2, which was previously suggested to play a restrictive role in postnatal development of central nervous system (CNS) vasculature (14, 17), showed early up-regulation (*S1PR2*, day 2: $P = 0.009$). Nogo-A mRNA levels remained constantly high in the ischemic border zone after stroke ($P = 0.993$). By immunofluorescence, Nogo-A was exclusively detected on nonvascular cells, whereas S1PR2 was localized to the vascular endothelium, including the motile tip cells that are required for angiogenesis, as was particularly evident in confocal images (Fig. 1*C*). Nogo-A and S1PR2 were not found in Nogo-A$^{-/-}$ and S1PR2$^{-/-}$ animals, demonstrating the specificity of the immunostaining, as has been described previously (18, 19).

These results show that the vascular repair in the periinfarct region is limited, leading to long-term hypoperfusion and further tissue damage. One mechanism for the limited vascular regrowth may be the presence of inhibitory factors including Nogo-A and its up-regulated receptor S1PR2 on motile vascular endothelial tip cells.

Genetic Deletion of Nogo-A or S1PR2 or Neutralization of Nogo-A by Antibodies Improves Vascular Repair and Network Formation but Does Not Attenuate Inflammatory or Scar-Forming Processes. To determine the influence of the Nogo-A pathway on vascular repair after stroke we took advantage of (*i*) constitutive Nogo-A knockout mice, (*ii*) S1PR2 knockout mice, and (*iii*) a function-blocking

anti–Nogo-A antibody (Ab) that was locally infused for 2 wk into the contralesional lateral ventricle (Fig. 2*A*). In wild-type (WT) animals 3 wk after stroke, an ischemic border zone characterized by severe hypovascularization extended up to 300 μm around the stroke core (Fig. 2*B*). Compared with the intact contralesional hemisphere, the vascular structure in this region was characterized by a significantly lower vascular area fraction (intact: 0.10 ± 0.01; lesioned: 0.06 ± 0.01, $P < 0.001$), decreased total length of blood vessels per square millimeter (intact: 57.74 ± 1.34 mm; lesioned: 31.88 ± 1.62 mm, $P < 0.001$), reduced number of branches per square millimeter (intact: 396.3 ± 5.21; lesioned: 126.56 ± 16.17, $P < 0.001$), increased nearest vessel neighbor distance (intact: 30.34 ± 0.48 μm, lesioned: 36.85 ± 1.09 μm, $P < 0.001$), and higher variability in the distribution of the blood vessels (10.28 ± 0.44 μm; lesioned: 15.55 ± 0.65 μm, $P < 0.001$) (Fig. 2 *B* and *C* and *SI Appendix*, Fig. S2*B*).

Both genetic knockouts Nogo-A$^{-/-}$ and S1PR2$^{-/-}$ showed a marked improvement in vascular repair, evident in all analyzed parameters. The effect was especially pronounced in the area fraction that was increased by +53% (S1PR2$^{-/-}$, $P = 0.032$) or +179% (Nogo-A$^{-/-}$, $P < 0.001$) and in the larger number of branches by +85% (S1PR2$^{-/-}$, $P = 0.028$) and +361% (Nogo-A$^{-/-}$, $P < 0.001$) compared with WT controls. Similar effects were observed in WT mice treated with anti–Nogo-A Ab: The vascular area fraction was increased by +102% ($P < 0.001$) and the number of branches by +436% ($P < 0.001$) compared with WT mice receiving isotype control antibodies (Fig. 2 *C* and *D* and *SI Appendix*, Fig. S3). Importantly, neither Nogo-A$^{-/-}$ nor S1PR2$^{-/-}$ nor anti–Nogo-A Ab-treated animals showed alterations in the vasculature of the contralesional hemisphere (all $P > 0.05$) or altered stroke volumes (all $P > 0.05$) (*SI Appendix*, Figs. S1 and S2).

Titers and functionality of anti–Nogo-A Ab were assessed by ELISA in serum samples. Anti–Nogo-A antibodies were detectable at all three time points in the serum of all mice in the treatment group: (*i*) during continuous intracerebroventricular Ab infusion on day 8, (*ii*) at the end of Ab administration on day 15, and (*iii*) before perfusion on day 22 (i.e., 7 d after the last infusion day). An increase of Ab titers during the 14-d administration period (day 8: anti–Nogo-A Abs 27.77 ± 3.06 μg/mL; day 15: 65.50 ± 15.82 μg/mL) was observed followed by a decrease thereafter (day 22: 34.49 ± 12.51 μg/mL; *SI Appendix*, Fig. S4). An amount of 42 μg/d (in total: 478 μg over 14 d) of anti–Nogo-A Abs was infused into the CNS (0.25 μL/h at a concentration of 7 mg/mL).

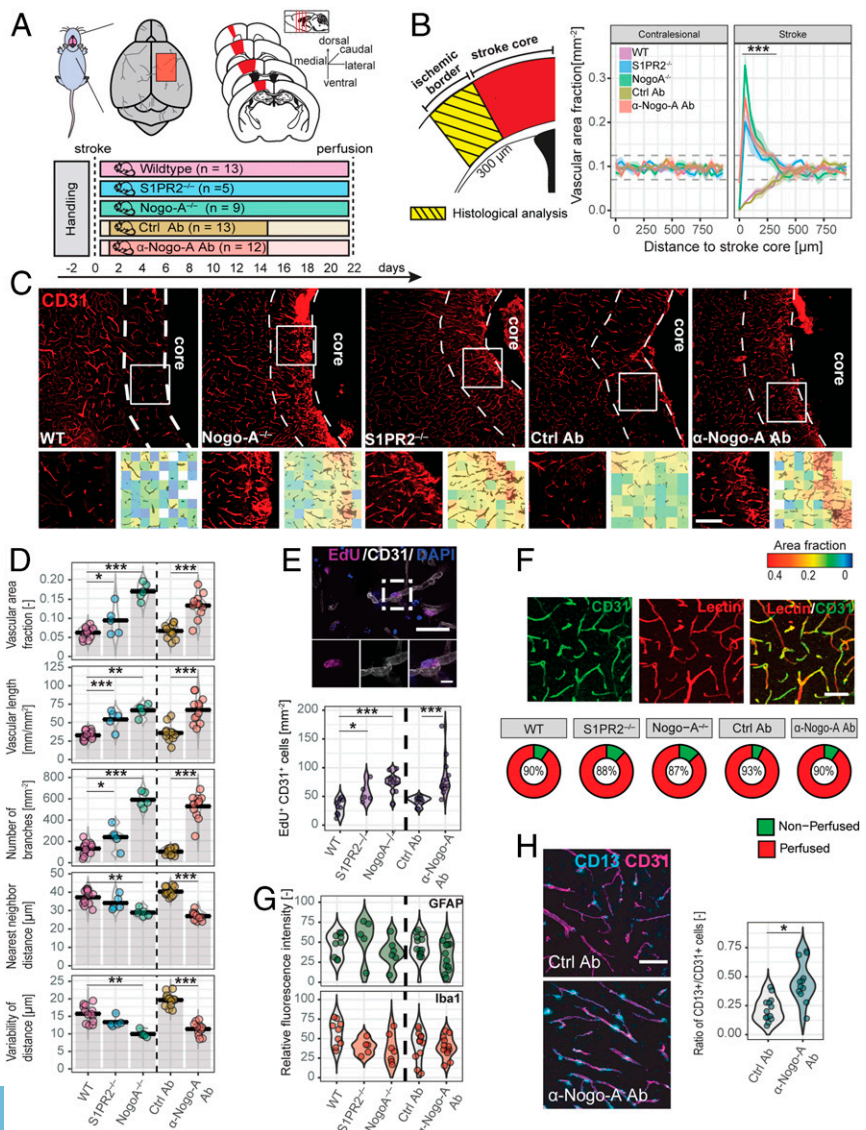

Fig. 2. Vascular repair in the ischemic border zone. (*A*) Schematic representation of the experimental timeline in the five experimental conditions: WT ($n = 13$), S1PR2$^{-/-}$ ($n = 5$), Nogo-A$^{-/-}$ ($n = 9$), Ctrl Ab ($n = 13$), and anti–Nogo-A Ab ($n = 12$). (*B*) Assessment of the vascular area fraction in the ipsilesional and contralesional sensory-motor cortex. (*C*) Blood vessels were visualized by CD31 immunostaining. Heat maps show the local area fraction of blood vessels in an area 0 to 300 μm from the stroke core. (Scale bars, 100 μm.) (*D*) Quantitative evaluation of the vascular area fraction, blood vessel length, number of branches, nearest-neighbor distance (NND), and variability of NND (SD NND) in the ischemic border zone of the different treatment groups. (*E*) Quantification of newly generated EdU^{+}/CD31^{+} endothelial cells. [Scale bars, 20 μm and 5 μm (zoom in).] (*F*) Ratio of perfused (red) to nonperfused (green) blood vessels in the five experimental groups. (Scale bars, 50 μm.) (*G*) Relative fluorescence intensity of GFAP and the microglia/macrophage marker Iba1. (*H*) Pericyte coverage assessed by the ratio of CD13^{+}/CD31^{+} cells. Data are mean ± SEM (one-way ANOVA with Dunnett's post hoc test). $^{*}P < 0.05$, $^{**}P < 0.01$, $^{***}P < 0.001$.

To address the origin of the blood vessels in the ischemic border zone, the nucleotide analog 5-ethynyl-2′-deoxyuridine (EdU) was systemically applied around the peak of poststroke angiogenesis at days 6, 7, and 8 (20). Three weeks after injury, we observed more newly formed blood vessels in Nogo-A$^{-/-}$ and S1PR2$^{-/-}$ mice in the ischemic border zone as indicated by a significant increase in the number of EdU^{+}/CD31^{+} cells per square millimeter (S1PR2$^{-/-}$: 56.52 ± 7.8, $P = 0.023$; Nogo-A$^{-/-}$: 75.31 ± 5.63, $P < 0.001$) compared with WT controls (33.05 ± 0.3.7). Similar results were observed by functional neutralization of Nogo-A (Ctrl Ab: 42.31 ± 2.1; anti–Nogo-A Ab: 83.00 ± 9.3, $P < 0.001$).

The functionality of the newly formed vessel network was assessed by the injection of a vascular tracer coupled to a fluorophore (Lectin-DyLight594) and laser Doppler flowmetry. Blood vessels were perfused to 87 to 93% in all tested conditions 3 wk after stroke (Fig. 2*F*). As therapeutic angiogenesis in the brain has previously been associated with immature vessels that lack stabilizing pericytes (21), we tested whether endothelial (CD31) and pericyte (CD13) markers were colocalized. We found that the pericyte coverage in the periinfarct region was higher in anti–Nogo-A Ab-treated animals (0.45 ± 0.029, $P = 0.018$) compared with controls (0.22 ± 0.03), suggesting a more mature vessel network. Interestingly, the degree of inflammation and scar formation, assessed by Iba1 and GFAP immunoreactivity, was comparable between all groups tested ($P > 0.05$) at 3 wk after stroke (Fig. 2 *G* and *H* and *SI Appendix*, Fig. S2 *D* and *E*).

We assessed in vivo blood perfusion in WT and Nogo-A–deficient animals around the stroke core by laser Doppler flowmetry (Fig. 3*A*). First, we confirmed that naïve cerebral blood perfusion levels did not differ between Nogo-A$^{-/-}$ and WT animals (*SI Appendix*, Fig. S5). Blood perfusion was partly restored in all regions except the stroke core over time in all groups. However, increased blood perfusion levels were found in several regions around the core in Nogo-A–deficient animals 21 d after injury. In particular, Nogo-A$^{-/-}$ sensorimotor regions associated with forelimb (region 3: +39%, $P = 0.042$; region 6: +85%, $P = 0.031$) and hindlimb (region 4: +62%, $P = 0.030$) function (22) showed improved blood perfusions compared with WT controls 3 wk after injury, suggesting that the newly formed vessels were functional and improving the local blood circulation in the periinfarct region (Fig. 3 *B* and *C*).

Overall, this indicates that targeting the Nogo-A pathway after stroke has a specific and local proangiogenic effect without markedly affecting immune or scar-forming processes in the periinfarct region.

Nogo-A– and S1PR2-Deleted Mice Have Improved Functional Outcome after Stroke That Correlates with Angiogenesis in the Ischemic Border Zone. Large destruction of the sensorimotor cortex by photothrombotic stroke causes marked deficits in the fore- and hindlimb motor function (23). To test whether the improved vascular repair observed after Nogo-A neutralization or Nogo-A deletion or S1PR2 deletion is relevant for functional recovery, motor performance was assessed in two behavioral settings at regular intervals for 3 wk (Fig. 4*A*). We determined the error rate of paw placements of the stroke-affected fore- and hindlimb on the irregular horizontal ladder and the paw preference, paw dragging, and paw symmetry in the cylinder test (24). Both tests showed a substantial deterioration of the performance 3 d postinjury with a partial recovery over time. All groups of animals had no differences in motor function at the prestroke baseline and acutely 3 d after stroke (all $P > 0.05$). A better performance in the cylinder test was detected 21 d after injury for the parameters paw dragging and symmetrical paw touches in the Nogo-A$^{-/-}$ and the S1PR2$^{-/-}$ animals as well as after Ab-mediated neutralization of Nogo-A (paw dragging (S1PR2$^{-/-}$: –36.1%, $P = 0.047$; Nogo-A$^{-/-}$: –63.0% $P = 0.001$; anti–Nogo-A Ab: –68.2%, $P < 0.001$ compared with their respective controls; symmetry of paw touches: S1PR2$^{-/-}$ +23.1%, $P = 0.368$; Nogo-A$^{-/-}$: +62.2% $P = 0.003$; anti–Nogo-A Ab: +58.4%, $P < 0.005$). No changes for the parameter paw preference could be detected between groups (Fig. 4*B*).

Differences in the recovery of forelimb function were also observed in the horizontal ladder task. S1PR2 and Nogo-A–deficient animals as well as anti–Nogo-A–treated animals showed fewer error touches per run (S1PR2$^{-/-}$: –35.9%, $P = 0.031$; Nogo-A$^{-/-}$: –49.1%, $P = 0.041$; anti–Nogo-A Ab: –34.3%, $P = 0.002$) compared with their respective controls 21 d after injury. Changes in hindlimb function were less pronounced. Only Nogo-A–deficient animals performed fewer hindlimb errors compared with their

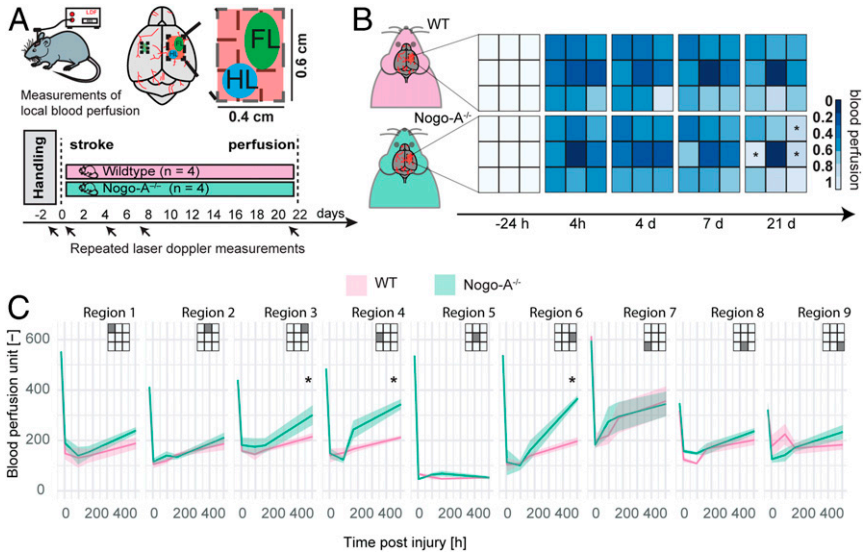

Fig. 3. Functional assessment of blood perfusion in the ischemic border zone by laser Doppler flowmetry. (*A*) Schematic representation of cerebral blood flow measurements in the same animal at sequential time points for WT ($n = 4$) and Nogo-A$^{-/-}$ (N = 4) animals after stroke. (*B*) Heat maps indicate local cerebral blood flow in nine subfields covering the stroke area. (*C*) Blood perfusion changes in forelimb- and hindlimb-related areas after stroke in Nogo-A$^{-/-}$ and WT animals. Data are mean ± SEM (Student's *t* test). *$P < 0.05$.

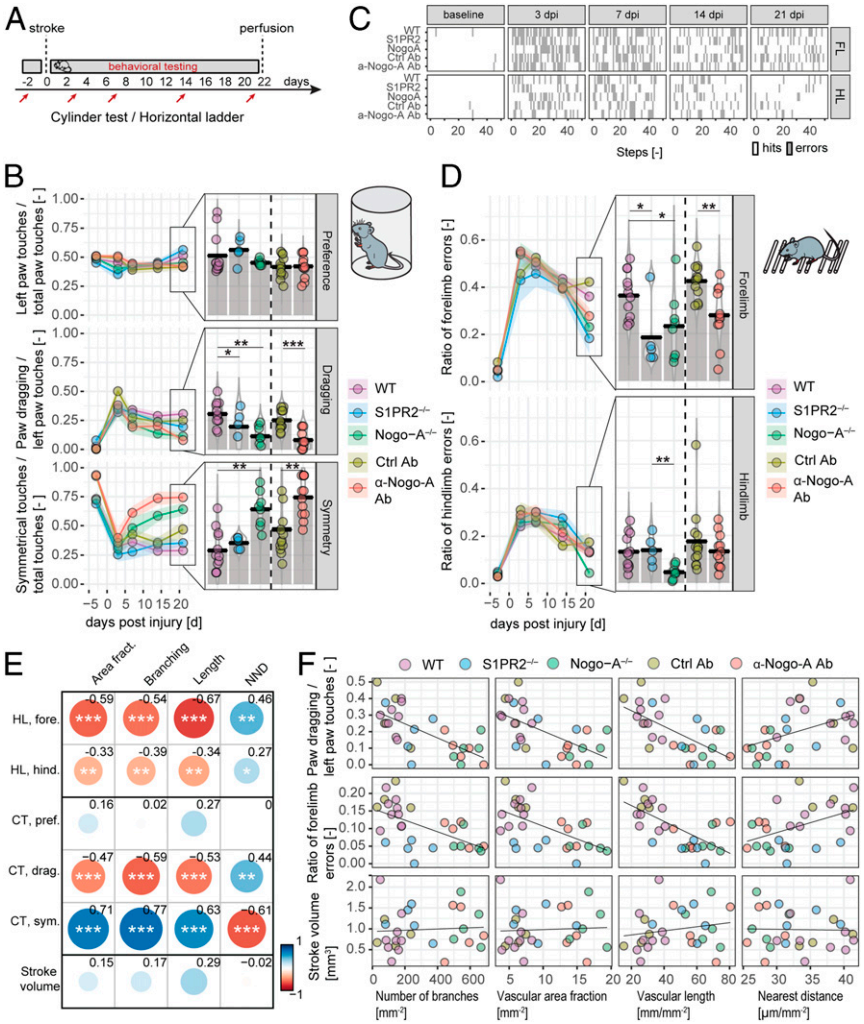

Fig. 4. Motor performance after photothrombotic stroke. (*A*) Timeline of behavioral testing after stroke. Motor performance of all animals was tested 3, 7, 14, and 21 d after stroke (arrows) in the horizontal ladder and cylinder test and compared with baseline performances. The groups consist of WT ($n = 13$), S1PR2$^{-/-}$ ($n = 5$), Nogo-A$^{-/-}$ ($n = 9$), Ctrl Ab ($n = 13$), and anti–Nogo-A Ab ($n = 12$). (*B*) Ratios of paw preference, dragging, and symmetry in the cylinder test. (*C*) Sequence of a horizontal ladder run with errors indicated by black bars from representative animals from each group. (*D*) Ratio of forelimb and hindlimb errors per total number of steps in the horizontal ladder test. (*E* and *F*) Correlation between motor function improvement and vascular parameters in single animals of WT, S1PR2$^{-/-}$, Nogo-A$^{-/-}$, Ctrl Ab, anti–Nogo-A Ab group 3 wk after stroke. Data are mean ± SEM (one-way ANOVA with Dunnett's post hoc test). $*P < 0.05$, $**P < 0.01$, $***P < 0.001$.

respective controls at 21 d postinjury (−66.1%, $P = 0.008$; Fig. 4*C*). Importantly, sham-operated animals did not change motor performance in any of the assessed tests (*SI Appendix*, Fig. S6).

Since all animals that underwent behavioral testing were also analyzed histologically, we correlated the behavioral improvements in both behavioral tests of each single animal to all of the vascular parameters from the periinfarct region. Importantly, we first confirmed that stroke volume did not correlate to any of the behavioral or vascular anatomy measures (Fig. 4*E*). In contrast, both functional outcomes correlated to a remarkable degree with the vascular repair. The strongest Pearson correlation was observed in paw dragging ($r = -0.59$, $P < 0.001$) and paw symmetry ($r = +0.77$, $P < 0.001$) in the cylinder test with vascular branching (Fig. 4 *E* and *F*).

These results indicate that inhibition of the Nogo-A pathway results in functional improvements 3 wk after stroke, which can be correlated with the vascular repair seen in the ischemic border zone.

Nogo-A Neutralization Improves Survival of Interneuronal Subtypes, Increases Specific Neurotransmitter Levels, and Reduces Apoptosis in the Ischemic Border Zone. We hypothesized that the restored blood flow and energy supply in the ischemic periinfarct zone may generate a permissive environment for protective and regenerative processes that could be responsible for the observed sensory-motor improvements. We first looked for a potential rescue effect on cortical neurons and levels of apoptosis. There was a marked 46% decrease of apoptotic caspase three-positive cells in animals treated with anti–Nogo-A antibodies (10.14 ± 0.95, $P = 0.004$) compared with controls (18.82 ± 2.79), although this was not reflected in the absolute number of cells expressing the neuronal marker NeuN per square millimeter (Ctrl Ab: 1,086.68 ± 142.57; anti–Nogo-A Ab: 1,216.99 ± 68.12, $P = 0.972$; Fig. 5 *A* and *B*).

With the metabolic differences of cortical neuron subtypes in mind, we next sought to look at neuronal subtypes that might be more susceptible or resilient to ischemia. GABAergic interneurons play an important role for perilesional plasticity and associated motor improvement after stroke (25, 26). We focused on

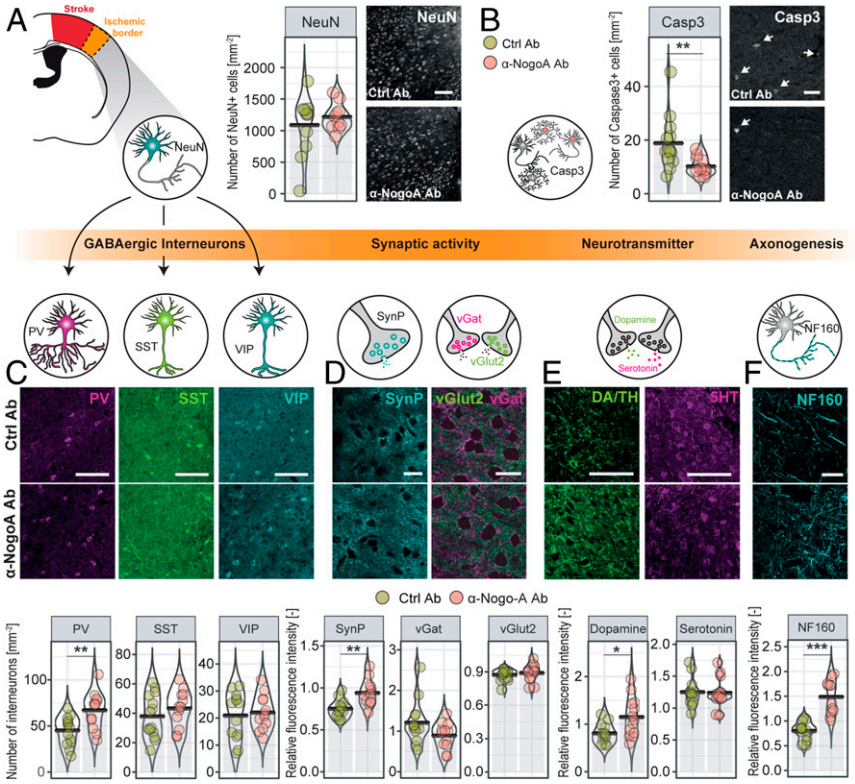

Fig. 5. Nonvascular effects of Nogo-A neutralization in the periinfarct zone 3 wk after stroke. The groups consist of animals receiving Ctrl Ab ($n = 13$) and anti–Nogo-A Ab ($n = 12$). (*A*) Number of NeuN$^+$ cells per mm^2. (Scale bar, 100 μm.) (*B*) Number of apoptotic cells positive for cleaved caspase 3 per mm^2 (Scale bar, 50 μm). (*C*) Numbers of PV$^+$, SST$^+$, and VIP$^+$ GABAergic interneurons per mm^2. (Scale bars, 100 μm.) (*D*) Relative fluorescence intensity of the synaptic markers synaptophysin, vGat and vGlut2. (Scale bars, 20 μm.) (*E*) Relative fluorescence intensity for TH/DA and 5-HT. (Scale bars, 100 μm.) (*F*) Relative fluorescence intensity of Nf160. (Scale bar, 20 μm.) Data are mean ± SEM (Student's *t* test). $*P < 0.05$, $**P < 0.01$, $***P < 0.001$.

three main subtypes that account for ∼85% of all cortical GABAergic interneurons (27): parvalbumin (PV)-, somatostatin (SST)-, and vasoactive intestinal peptide (VIP)-expressing cells. Quantification 21 d after stroke revealed an overall but unequal loss of interneurons: PV-positive cells: −64%, SST-positive cells: −55%, and VIP-positive cells: −16% compared with the intact cortex (intact: PV: 116.22 ± 14.54, SST: 85.01 ± 12.29, VIP: 24.9 ± 4.45; stroked: PV: 45.33 ± 2.95, SST: 38.26 ± 2.82, VIP: 20.94 ± 1.68). Interestingly, in the anti–Nogo-A Ab-treated animals the loss of PV-positive interneurons was partially rescued to 50% (Ctrl Ab: 45.33 ± 2.95; anti–Nogo-A Ab: 68.21 ± 4.02, $P = 0.003$). No differences in the number of the other two GABAergic interneuron subtypes SST (Ctrl Ab: 38.26 ± 2.82; anti–Nogo-A Ab: 43.94 ± 2.54, $P = 0.286$) and VIP (Ctrl Ab: 20.94 ± 1.68; anti–Nogo-A Ab: 22.04 ± 1.29, $P = 0.806$) were detected (Fig. 5*C*).

To investigate synaptic changes, immunostaining was performed in the periinfarct region for three synaptic markers: synaptophysin localized in presynaptic vesicles and the vesicular glutamate and GABA transporters vGlut2 and vGat, expressed in synaptic vesicles of glutamatergic or GABAergic neurons, respectively. Compared with the contralesional side, synaptophysin immunoreactivity was decreased by −25%, suggesting a loss of synapses 3 wk after stroke in the ischemic border zone. This loss was much lower in the ischemic zone of anti–Nogo-A treated animals ($P = 0.003$), reaching 94% of intact cortical synaptophysin expression. Quantitative analysis of vGlut2 and vGat expression revealed a decrease of −13% for vGlut2 and an increase of 20% for vGat in the ischemic border zone compared with intact cortical regions 3 wk after stroke. However, no changes were observed when comparing control and anti–Nogo-A Ab-treated animals (vGat: $P = 0.192$; vGlut: $P = 0.369$; Fig. 5*D*).

Neurotransmitters shown to play key roles in motor learning, function, and recovery are dopamine (DA) and serotonin (5-HT). Areal optical density measurements after immunostaining for tyrosine hydroxylase, an enzyme required for DA synthesis, or 5-HT showed a decrease of 19.2% for DA and increase of 23% for 5-HT 21 d after stroke compared with the intact sensory-motor cortex. In anti–Nogo-A Ab-treated stroke cortices, DA levels were found to be significantly higher (42.2%, $P = 0.029$) than in the stroked controls, whereas 5-HT levels did not significantly change between the groups ($P = 0.892$; Fig. 5*E*).

Importantly, we also observed that anti–Nogo-A treatment promoted the growth of axons within the ischemic border zone. Utilizing Neurofilament 160 (Nf160) as a marker, we assessed the optical axon density in the perilesional area. Three weeks after stroke the density of axons decreased to 20% compared with intact cortex. However, animals receiving anti–Nogo-A Ab had 83% ($P < 0.001$) more fibers in the ischemic border zone compared with their controls (Fig. 5*F*).

These results show that the restored vascular circulation induced by Nogo-A neutralization results in protective and regenerative neuronal processes in the ischemic border zone.

Blocking VEGF-Mediated Angiogenesis Decreases the Beneficial Effects of Nogo-A Deletion. Since Nogo-A is known to be an important inhibitor of axonal remodeling (28, 29), it was uncertain to what extent functional improvements could be directly linked to improved vascular repair in the ischemic border zone. To test this, we systemically blocked VEGF-mediated angiogenesis in Nogo-A$^{-/-}$ mice using an anti-VEGF Ab (Avastin; Roche) after

stroke and examined these animals for functional recovery in the ladder walk and the cylinder test (WT_{AV} and Nogo-$A^{-/-}{}_{AV}$) as characterized before. Control groups received FG12, a control Ab (WT_{CTRL} and Nogo-$A^{-/-}{}_{CTRL}$) (Fig. 6*A*).

As expected, we observed a decrease in vascular area fraction (−41.8%, $P = 0.020$), vascular length (−30.9%, $P = 0.083$), and branching (−63.0%, $P = 0.006$) in Avastin-treated Nogo-$A^{-/-}{}_{AV}$ animals compared with their Nogo-$A^{-/-}{}_{CTRL}$ controls. Interestingly, all these vascular parameters were also decreased in WT_{AV} animals, suggesting the presence of limited spontaneous, VEGF-dependent angiogenesis also in WT animals after stroke (Fig. 6*B*). The number of newly formed blood vessels was reduced by half in Nogo-$A^{-/-}{}_{AV}$ (−56.5%, $P < 0.001$) as well as WT_{AV} (−56.7%, $P = 0.010$) compared with control Ab-treated animals (Fig. 6*B*). Quantification of $EdU^+/CD31^+$ cells showed that endothelial proliferation was equally reduced (Fig. 6*C*). Importantly, the stroke volumes were comparable in all tested groups (*SI Appendix*, Fig. S7).

To test whether the reduction of poststroke angiogenesis in the periinfarct regions by anti-VEGF affects the behavioral outcome, we tested Nogo-A and WT animals that received either Avastin or the control Ab, respectively, in the same behavioral tasks as described before (Fig. 6*A*). The results from the horizontal irregular ladder (foot placement error rate) and the cylinder test confirmed the results from the previous study: Nogo-$A^{-/-}{}_{CTRL}$ animals performed significantly better in both behavioral tasks than their WT_{CTR}L 3 wk after injury (Fig. 6 *D* and *E*). This reduction in the error misstep rates on the horizontal ladder was abolished in the Nogo-$A^{-/-}{}_{AV}$ group (8.8 ± 1.1%, $P = 0.003$) compared with the Nogo-$A^{-/-}{}_{CTRL}$ controls (0.3 ± 0.2%) and similar to the WT groups (WT_{CTRL}: 5.5 ± 0.7%; WT_{AV}: 7.2 ± 0.7%) (Fig. 6*D*). A similar pattern was observed in the cylinder test. Nogo-$A^{-/-}{}_{AV}$ animals had an increased ratio of dragging to total paw touches compared with the control group (Nogo-$A^{-/-}{}_{CTRL}$: 0.11 ± 0.04; Nogo-$A^{-/-}{}_{AV}$: 0.34 ± 0.03, $P = 0.005$; Fig. 6*E*).

These observations suggest that neutralization of VEGF abolishes the beneficial effect of Nogo-A deletion and that periinfarct angiogenesis plays an important role for certain behavioral improvements after stroke.

In Vitro Vessel Formation by Human Umbilical Vein Vascular Endothelial Cells Is Limited by Nogo-A in a 3D Glycosaminoglycan-Poly(Ethylene Glycol) Hydrogel Model. Three-dimensional cultures of human umbilical vein vascular endothelial cells (HUVECs) in defined hydrogels represent a valuable tool to study capillary network formation in vitro, eliminating the impact of signaling from surrounding tissues observed in in vivo studies (30). To investigate the effect of Nogo-A in such a minimalistic setup, we have embedded HUVECs in a glycosaminoglycan-based biohybrid hydrogel supplemented with the vascular growth factors VEGF, SDF1, and FGF2, which has been shown to effectively promote HUVEC vessel formation (31) (Fig. 7*A*). Within 3 d of culture, extensive, branched, and anastomosing vessel-like capillary networks formed. To assess whether Nogo-A also inhibits vascular growth in the presence of growth factors in vitro we have added crude myelin extract known to contain Nogo-A (31) to the hydrogel culture. Vascular growth was inhibited by ∼60%, as reflected by all of the measured vascular parameters (area fraction: −56.1%; vascular diameter: −66.8%; number of branches: −57.7%; vascular length: −52.4%, all $P < 0.001$). Vessel growth could be partially rescued by the addition of a neutralizing anti–Nogo-A Ab as evidence by an increase in vascular area (+41.0%,

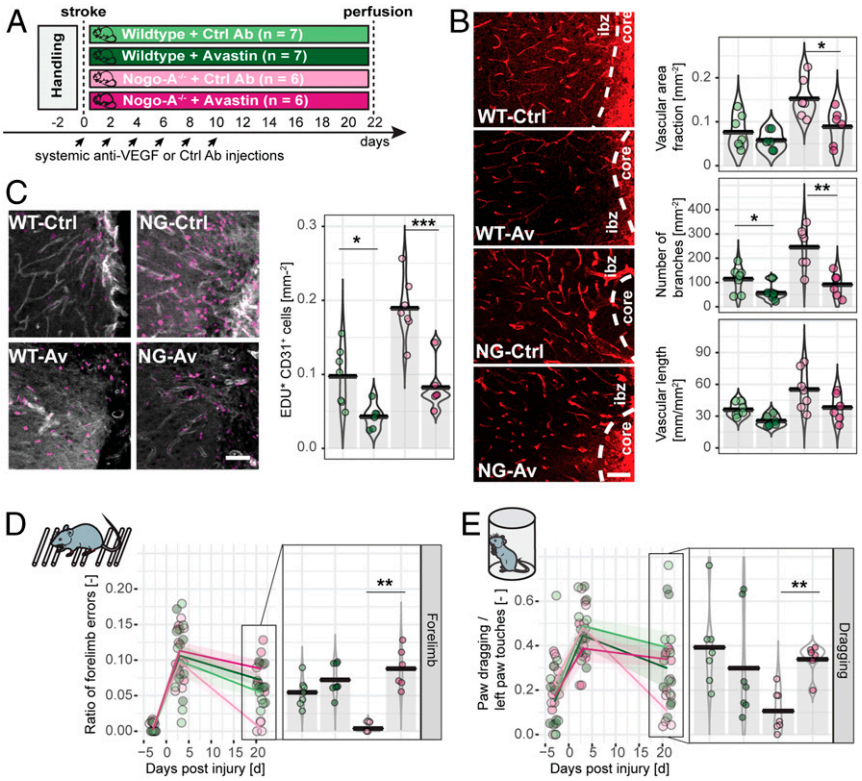

Fig. 6. Reduction of angiogenesis in the periinfarct region by anti-VEGF reduces the functional recovery effects of Nogo-A deletion. (*A*) Experimental timeline after stroke. WT or Nogo-A KO animals received either anti-VEGF (Avastin, Av; arrows) or a control Ab (Ctrl) i.v. every other day for 10 d after stroke. (*B*) Assessment of the vascular area fraction, vascular length and number of branches in the periinfarct region. (Scale bar, 20 μm.) (*C*) Quantification of $EdU^+/CD31^+$ cells. (Scale bars, 20 μm.) (*D* and *E*) Behavioral performance assessed at baseline and 3, 7, 14, and 21 d postinjury in the horizontal ladder (*D*) and cylinder test (*E*). Data are mean ± SEM (one-way ANOVA with Dunnett's post hoc test). *$P < 0.05$, **$P < 0.01$, ***$P < 0.001$.

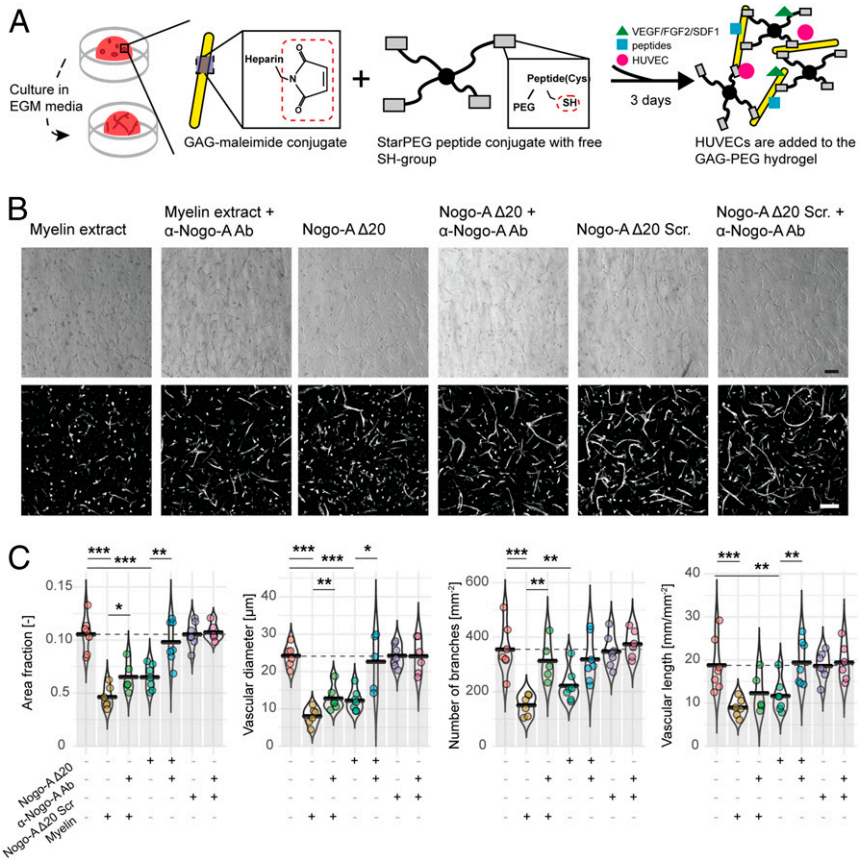

Fig. 7. Vessel and capillary network formation by HUVECs in vitro is limited by CNS myelin and Nogo-A in a 3D GAG-PEG hydrogel model. (*A*) Schematic overview of the in situ assembly of GAG-PEG gel-based 3D cultures from reactive polymer conjugates, HUVECs, and heparin-binding growth factors (VEGF, FGF2, and SDF1). (*B*) Bright-field and fluorescent images of tubular network formation by HUVECs ($CD31^+$) in GAG-PEG hydrogels supplemented with the neurite growth inhibitory Nogo-A domain Nogo-A Δ20, the neutralizing Nogo-A Ab 11C7, scrambled Nogo-A Δ20, or CNS myelin extract. (Scale bar, 100 μm.) (*C*) Quantification of area fraction, diameter, branch number, and length of HUVEC-derived vessels (n = 5 to 7 cultures). Data are mean ± SEM (one-way ANOVA with Dunnett's post hoc test). $^*P < 0.05$, $^{**}P < 0.01$, $^{***}P < 0.001$.

$P = 0.044$), an increased number of vascular branches (+108.6%, $P = 0.002$), and vascular diameter (+59.0%, $P = 0.002$) compared with myelin-exposed HUVECs (Fig. 7 *B* and *C*). These data show that crude myelin extracts significantly inhibit vessel formation in vitro in a Nogo-A–dependent way.

To gain more insight into the protein domain responsible for this effect we added the Nogo-A inhibitory fragment Nogo-A Δ20 to the culture (19). Nogo-A Δ20 substantially inhibited vessel formation as reflected by all of the measured vascular parameters (area fraction −38.4%, $P < 0.001$; diameter: −49.7%, $P < 0.001$; branches: −37.5%, $P = 0.002$; length: −38.0%, $P = 0.003$), which suggests that Nogo-A limits angiogenesis despite the presence of growth factors with critical involvement of its Nogo-A Δ20 domain. The addition of anti–Nogo-A antibodies known to block the Nogo-A Δ20 activity (19) partly rescued the HUVEC network formation (Fig. 7 *B* and *C*) and improved vascular growth in all vascular measures, especially in the average diameter of the blood vessels (+85.8%, $P = 0.032$) and vascular length (+66.7%, $P = 0.008$). Importantly, the addition of scrambled Nogo A Δ20 peptide as well as the Δ20 activity-blocking Ab alone did not influence the vascular network formation (Fig. 7 *B* and *C*).

These data confirm the inhibitory function of Nogo-A on angiogenesis and show that the Nogo-A fragment Δ20 plays an important inhibitory role in vessel formation. Targeting this domain with neutralizing antibodies may thus represent a promising clinical approach to improve vascular repair in ischemic diseases.

Discussion

Brain tissue lost due to severe ischemia has a very limited capacity to spontaneously regenerate, resulting in a cavity with a sparse, disordered vasculature. This results in a hypoperfused ischemic boundary region, which gradually evolves into infarction in the absence of reperfusion and is associated with permanent functional deficits in stroke patients. Clinically, treatments to enhance poststroke angiogenesis, for example by VEGF (8), are lacking or not feasible, mainly due to side effects, despite preclinical evidence for beneficial effects (7). The present results show that genetic deletion of Nogo-A or its receptor subunit S1PR2 or Ab-mediated neutralization of Nogo-A results in strong stimulation of blood vessel regrowth in the periinfarct region of adult mice with large cortical strokes. The restored, perfused vascular bed promoted survival and repair of critical neuronal subpopulations and fiber systems and was correlated with enhanced motor recovery. Vessel growth and behavioral recovery were lost when the enhanced angiogenic response was blocked by anti-VEGF antibodies.

The recognition that higher levels of angiogenesis correlate with improved functional recovery in animal models and stroke patients represents a therapeutic option for ischemic stroke (4). In an attempt to enhance vascular repair, most studies have focused on the prototypical angiogenic mediator VEGF. However, the delivery of recombinant VEGF showed considerable side effects, as it worsened edema and raised the risk for hemorrhages through its enhancement of vascular permeability and the

fragility of the immature, sprouted vessels (8). VEGF negatively regulates vascular maturation and stabilization by ablating pericyte coverage of nascent vascular sprouts (32). These destabilizing effects were shown to be mediated through RhoA/ROCK signaling, whose regulation of cell motility, proliferation, survival, and permeability is well-characterized (33). Thus, alternative strategies beyond VEGF like the delivery or inhibition of guidance factors have attracted attention in the field of angiogenic therapy. Interestingly, the inhibitory effects of Nogo-A on brain endothelial cells are mediated by intracellular RhoA activation through the receptor S1PR2 (17, 18). Nogo-A blockage may, therefore, reduce RhoA activation and thus promote tip cell migration and reduce BBB leakage, both by decreasing Rho/ROCK activation. We found that anti–Nogo-A Abs stimulated vascular structures with pericyte coverage, which are important for stabilization and maturation of newly formed blood vessels (34, 35). No evidence was found for an increase of stroke size or inflammatory $Iba1^+$ cell activation as previously associated with VEGF therapy (36). Our results in the in vitro model further indicate that the presence of growth factors alone might not be sufficient to establish a robust vascular network at mutual presence of inhibitory factors including Nogo-A. We propose a similar process in the pathophysiological conditions after stroke, where inhibitory factors including Nogo-A are present (28).

Findings from a growing number of studies suggest that improved angiogenesis supports tissue preservation and repair, leading to functional improvement. However, angiogenesis has rarely been directly tested for its role in behavioral recovery (37). In the present study, we show that the functional improvements generated through Nogo-A neutralization are abolished when VEGF-mediated angiogenesis is inhibited in the periinfarct regions, indicating their dependence on vascular repair. Although numerous in vitro studies have shown a direct and independent inhibitory effect of Nogo-A on growth of both neuronal axons (19) and vascular endothelial cells (14), it is experimentally challenging to completely uncouple neuro- and angiogenic effects in vivo due to the mutual influence of both systems on each other. Enhanced motor recovery has been previously observed in stroked rats under anti–Nogo-A Ab treatment, which was abolished by silencing the sprouted corticospinal fibers from the intact hemisphere (29). Similarly, functional recovery was improved by local injection of angiogenic biomaterials that promoted revascularization following stroke. The beneficial behavioral effects were blocked by either blocking angiogenesis or silencing the newly formed axonal network in the periinfarct regions (37). Thus, we think that both mechanisms, vascular repair and neural sprouting, may act in conjunction. Advancements in genetic models and in vivo microscopy may help to further dissect the vascular form the neuronal plastic effects and their contribution to specific aspects of functional recovery in future studies.

To investigate the underlying function-improving effects of Nogo-A neutralization, we studied several classes of cells known to be associated with repair and plasticity processes after stroke. Within the region of improved vascular repair we observed fewer apoptotic cells accompanied by an increase in the number of PV^+ GABAergic interneurons that have been shown to play key roles in cortical activity networks including learning and other activity-dependent plasticity paradigms (38–40). Furthermore, we observed an increase in expression of synaptic marker (synaptophysin), indicating that Nogo-A neutralization may facilitate aspects of synaptic activity or synaptic density that may enhance the susceptibility of the lesioned brain to adaptive change and recovery. In addition, dopamine, a neurotransmitter essentially involved in cortical synaptic plasticity and motor skill learning (41, 42), was increased. Axonal density was significantly higher after Nogo-A neutralization in the ischemic border zone, but further studies are required to analyze if these are newly formed axonal sprouts or surviving axons and how they contribute to functional improvement.

All these findings suggest that the ischemic perilesional tissue undergoes reduced degenerative changes due to the early revascularization and that anti–Nogo-A antibodies also enhance sprouting and reconnectivity in this metabolically stabilized tissue. From a clinical perspective, a treatment that combines beneficial regenerative effects on both the vascular and neuronal network would seem highly advantageous for the promotion of functional recovery in stroke patients.

Nogo-B, another isoform of the Nogo/RTN4 family, and its receptor NgBR have been shown to promote angiogenesis in several non-CNS tissues (43, 44). Here, Nogo-B was found to be up-regulated in the periinfarct region of WT animals and has also been previously reported to be activated following Nogo-A deletion (45). Although no function of Nogo-B in the ischemic CNS has been recognized so far, we cannot exclude its participation in the proangiogenic effect in our studies using conventional Nogo-A–deficient animals. However, the finding that animals lacking S1PR2, the Nogo-A–specific receptor in endothelial cells, also had improved vascular parameters suggests that Nogo-A signaling significantly contributes to vascular impairment. This is in accordance with in vitro findings from previous and the current study indicating that the Nogo-A Δ20 active domain but not Nogo-66 inhibits sprouting and migration of vascular cells through the S1PR2 receptor (14, 17, 18).

From a therapeutic perspective, it might be even beneficial if Ab-targeted Nogo-A neutralization may support other proangiogenic signaling cascades including Nogo-B.

Besides Nogo-A suppression, similar beneficial effects have been shown for other guidance molecules in a number of preclinical studies for CNS ischemia. For example, viral overexpression of the positive guidance molecule Netrin1 promoted angiogenesis and long-term neurological recovery in a mouse model of transient focal ischemia (46). Also, activation of the guidance molecule ephrinB2 enhanced neurovascular repair and pericyte recruitment after brain ischemia (47). On the other hand, inhibition of the repulsive axonal guidance molecule Semaphorin 4D reduced BBB permeability as well as infarct volume and improved neurologic performance of rats after transient middle cerebral artery occlusion (48).

Guidance cue-targeted therapies may also ameliorate vascular disease in the retina, as intravitreal administration of Semaphorin 3A blocked misguided neovascularization in a mouse model of oxygen-induced retinopathy (49, 50). In the same mouse model, intravitreal application of anti–Nogo-A Abs markedly inhibited neovascular tuft formation, enhanced the vascularization of deep retinal layers, and improved visual function (15). These findings together with our present data suggest that therapeutic interventions targeting repulsive guidance cues, in particular Nogo-A, might be a promising strategy to promote functional angiogenesis in ischemic CNS conditions. Indeed, safety and feasibility of intrathecal anti–Nogo-A Ab delivery have recently been demonstrated in a phase I clinical trial for spinal cord injury (51).

Materials and Methods

The goal of the present study was to test if blockage of the neurite outgrowth inhibitor Nogo-A improves vascular repair in mice with cerebral ischemia. We hypothesized that high Nogo-A levels restrict the formation of new blood vessels in the ischemic border zone, similar to its previously reported role in negative regulation of developmental CNS vasculature (14). Its inhibition may facilitate the generation of a more permissive environment for neuroprotective and regenerative processes that ultimately might result in improved function.

To test this, we first test genetic mouse models deficient for Nogo-A ($n = 9$) or its corresponding receptor S1PR2 ($n = 5$) or neutralized Nogo-A with a function-blocking anti–Nogo-A Ab ($n = 12$). Control animals in all experiments were WT littermates ($n = 13$) or animals receiving an IgG isotype control Ab ($n = 13$). We assessed motor skills of the stroked animals at baseline and at 3, 7, 14, and 21 d after injury (52). Ischemic cortical tissue was histologically

analyzed after 3 wk for vascular function (53), cell survival, synaptic and neurotransmitter activity, and regenerative processes. A subset of Nogo-A$^{-/-}$ and WT animals underwent functional blood perfusion analysis with laser Doppler flowmetry (n = 4 per group). To link improved vascular repair with functional improvement after Nogo-A blockage, we blocked poststroke angiogenesis of Nogo-A$^{-/-}$ mice by systemic application of anti-VEGF antibodies for 10 d after stroke (n = 6 to 7 per group). Moreover, in an in vitro 3D hydrogel model we tested the effects of Nogo-A components together with VEGF on the vascular network (54, 55) (n = 5 to 7 per group).

All animals are presented in the study; no statistical outliers were excluded. Data were acquired blinded. The surgery, behavioral testing and analysis of the data were performed by different investigators that were blinded in all steps of analysis.

All experiments were conducted in accordance with the applicable national regulations and approved by the Cantonal Veterinary Department of Zurich.

For a detailed description of these topics, see *SI Appendix, SI Materials and Methods*.

1. E. J. Benjamin *et al*.; American Heart Association Statistics Committee and Stroke Statistics Subcommittee, Heart disease and stroke statistics-2017 update: A report from the American Heart Association. *Circulation* **135**, e146–e603 (2017). Correction in: *Circulation* **136**, e196 (2017).
2. V. L. Feigin *et al*.; Global Burden of Diseases, Injuries and Risk Factors Study 2013 and Stroke Experts Writing Group, Global burden of stroke and risk factors in 188 countries, during 1990-2013: A systematic analysis for the Global Burden of Disease Study 2013. *Lancet Neurol.* **15**, 913–924 (2016).
3. R. D. Henderson, M. Eliasziw, A. J. Fox, P. M. Rothwell, H. J. Barnett; North American Symptomatic Carotid Endarterectomy Trial (NASCET) Group, Angiographically defined collateral circulation and risk of stroke in patients with severe carotid artery stenosis. *Stroke* **31**, 128–132 (2000).
4. J. Krupinski, J. Kaluza, P. Kumar, S. Kumar, J. M. Wang, Role of angiogenesis in patients with cerebral ischemic stroke. *Stroke* **25**, 1794–1798 (1994).
5. T. Hayashi, N. Noshita, T. Sugawara, P. H. Chan, Temporal profile of angiogenesis and expression of related genes in the brain after ischemia. *J. Cereb. Blood Flow Metab.* **23**, 166–180 (2003).
6. M. Navarro-Sobrino *et al*., A large screening of angiogenesis biomarkers and their association with neurological outcome after ischemic stroke. *Atherosclerosis* **216**, 205–211 (2011).
7. A. Ergul, A. Alhusban, S. C. Fagan, Angiogenesis: A harmonized target for recovery after stroke. *Stroke* **43**, 2270–2274 (2012).
8. Z. G. Zhang *et al*., VEGF enhances angiogenesis and promotes blood-brain barrier leakage in the ischemic brain. *J. Clin. Invest.* **106**, 829–838 (2000).
9. R. H. Adams, A. Eichmann, Axon guidance molecules in vascular patterning. *Cold Spring Harb. Perspect. Biol.* **2**, a001875 (2010).
10. P. Carmeliet, M. Tessier-Lavigne, Common mechanisms of nerve and blood vessel wiring. *Nature* **436**, 193–200 (2005).
11. R. Rust, C. Gantner, M. E. Schwab, Pro- and antiangiogenic therapies: Current status and clinical implications. *FASEB J.* **33**, 34–48 (2019).
12. H. Gerhardt *et al*., VEGF guides angiogenic sprouting utilizing endothelial tip cell filopodia. *J. Cell Biol.* **161**, 1163–1177 (2003).
13. O. I. Kahn, P. W. Baas, Microtubules and growth cones: Motors drive the turn. *Trends Neurosci.* **39**, 433–440 (2016).
14. T. Wälchli *et al*., Nogo-A is a negative regulator of CNS angiogenesis. *Proc. Natl. Acad. Sci. U.S.A.* **110**, E1943–E1952 (2013).
15. S. Joly, A. Dejda, L. Rodriguez, P. Sapieha, V. Pernet, Nogo-A inhibits vascular regeneration in ischemic retinopathy. *Glia* **66**, 2079–2093 (2018).
16. A. M. Buga *et al*., Transcriptomics of post-stroke angiogenesis in the aged brain. *Front. Aging Neurosci.* **6**, 44 (2014).
17. G. S. Kim *et al*., Critical role of sphingosine-1-phosphate receptor-2 in the disruption of cerebrovascular integrity in experimental stroke. *Nat. Commun.* **6**, 7893 (2015).
18. A. Kempf *et al*., The sphingolipid receptor S1PR2 is a receptor for Nogo-a repressing synaptic plasticity. *PLoS Biol.* **12**, e1001763 (2014).
19. T. Oertle *et al*., Nogo-A inhibits neurite outgrowth and cell spreading with three discrete regions. *J. Neurosci.* **23**, 5393–5406 (2003).
20. M. Slevin *et al*., Serial measurement of vascular endothelial growth factor and transforming growth factor-beta1 in serum of patients with acute ischemic stroke. *Stroke* **31**, 1863–1870 (2000).
21. Y. Ma, A. Zechariah, Y. Qu, D. M. Hermann, Effects of vascular endothelial growth factor in ischemic stroke. *J. Neurosci. Res.* **90**, 1873–1882 (2012).
22. A. Sigler, M. H. Mohajerani, T. H. Murphy, Imaging rapid redistribution of sensory-evoked depolarization through existing cortical pathways after targeted stroke in mice. *Proc. Natl. Acad. Sci. U.S.A.* **106**, 11759–11764 (2009).
23. M. Balkaya, J. M. Kröber, A. Rex, M. Endres, Assessing post-stroke behavior in mouse models of focal ischemia. *J. Cereb. Blood Flow Metab.* **33**, 330–338 (2013).
24. R. B. Roome, J. L. Vanderluit, Paw-dragging: A novel, sensitive analysis of the mouse cylinder test. *J. Vis. Exp.*, e52701 (2015).
25. A. N. Clarkson, B. S. Huang, S. E. MacIsaac, I. Mody, S. T. Carmichael, Reducing excessive GABA-mediated tonic inhibition promotes functional recovery after stroke. *Nature* **468**, 305–309 (2010).
26. T. Hiu *et al*., Enhanced phasic GABA inhibition during the repair phase of stroke: A novel therapeutic target. *Brain* **139**, 468–480 (2016).
27. B. Rudy, G. Fishell, S. Lee, J. Hjerling-Leffler, Three groups of interneurons account for nearly 100% of neocortical GABAergic neurons. *Dev. Neurobiol.* **71**, 45–61 (2011).
28. J. L. Cheatwood, A. J. Emerick, M. E. Schwab, G. L. Kartje, Nogo-A expression after focal ischemic stroke in the adult rat. *Stroke* **39**, 2091–2098 (2008).
29. A. S. Wahl *et al*., Neuronal repair. Asynchronous therapy restores motor control by rewiring of the rat corticospinal tract after stroke. *Science* **344**, 1250–1255 (2014).
30. K. Chwalek, L. J. Bray, C. Werner, Tissue-engineered 3D tumor angiogenesis models: Potential technologies for anti-cancer drug discovery. *Adv. Drug Deliv. Rev.* **79–80**, 30–39 (2014).
31. K. Chwalek, M. V. Tsurkan, U. Freudenberg, C. Werner, Glycosaminoglycan-based hydrogels to modulate heterocellular communication in in vitro angiogenesis models. *Sci. Rep.* **4**, 4414 (2014).
32. J. I. Greenberg *et al*., A role for VEGF as a negative regulator of pericyte function and vessel maturation. *Nature* **456**, 809–813 (2008).
33. B. A. Bryan *et al*., RhoA/ROCK signaling is essential for multiple aspects of VEGF-mediated angiogenesis. *FASEB J.* **24**, 3186–3195 (2010).
34. K. Kisler *et al*., Pericyte degeneration leads to neurovascular uncoupling and limits oxygen supply to brain. *Nat. Neurosci.* **20**, 406–416 (2017).
35. A. Montagne *et al*., Pericyte degeneration causes white matter dysfunction in the mouse central nervous system. *Nat. Med.* **24**, 326–337 (2018).
36. S. D. Croll *et al*., VEGF-mediated inflammation precedes angiogenesis in adult brain. *Exp. Neurol.* **187**, 388–402 (2004).
37. L. R. Nih, S. Gojgini, S. T. Carmichael, T. Segura, Dual-function injectable angiogenic biomaterial for the repair of brain tissue following stroke. *Nat. Mater.* **17**, 642–651 (2018).
38. E. Favuzzi *et al*., Activity-dependent gating of parvalbumin interneuron function by the perineuronal net protein brevican. *Neuron* **95**, 639–655.e10 (2017).
39. F. Donato, S. B. Rompani, P. Caroni, Parvalbumin-expressing basket-cell network plasticity induced by experience regulates adult learning. *Nature* **504**, 272–276 (2013).
40. O. Caillard *et al*., Role of the calcium-binding protein parvalbumin in short-term synaptic plasticity. *Proc. Natl. Acad. Sci. U.S.A.* **97**, 13372–13377 (2000).
41. J. A. Hosp, A. Pekanovic, M. S. Rioult-Pedotti, A. R. Luft, Dopaminergic projections from midbrain to primary motor cortex mediate motor skill learning. *J. Neurosci.* **31**, 2481–2487 (2011).
42. K. Molina-Luna *et al*., Dopamine in motor cortex is necessary for skill learning and synaptic plasticity. *PLoS One* **4**, e7082 (2009).
43. J. Yu *et al*., Reticulon 4B (Nogo-B) is necessary for macrophage infiltration and tissue repair. *Proc. Natl. Acad. Sci. U.S.A.* **106**, 17511–17516 (2009).
44. R.-J. Teng *et al*., Nogo-B receptor modulates angiogenesis response of pulmonary artery endothelial cells through eNOS coupling. *Am. J. Respir. Cell Mol. Biol.* **51**, 169–177 (2014).
45. M. Simonen *et al*., Systemic deletion of the myelin-associated outgrowth inhibitor Nogo-A improves regenerative and plastic responses after spinal cord injury. *Neuron* **38**, 201–211 (2003).
46. H. Lu *et al*., Netrin-1 hyperexpression in mouse brain promotes angiogenesis and long-term neurological recovery after transient focal ischemia. *Stroke* **43**, 838–843 (2012).
47. A. Ghori *et al*., EphrinB2 activation enhances vascular repair mechanisms and reduces brain swelling after mild cerebral ischemia. *Arterioscler. Thromb. Vasc. Biol.* **37**, 867–878 (2017).
48. Y.-F. Zhou *et al*., Sema4D/PlexinB1 inhibition ameliorates blood-brain barrier damage and improves outcome after stroke in rats. *FASEB J.* **32**, 2181–2196 (2018).
49. Y. Fukushima *et al*., Sema3E-PlexinD1 signaling selectively suppresses disoriented angiogenesis in ischemic retinopathy in mice. *J. Clin. Invest.* **121**, 1974–1985 (2011).
50. J.-S. Joyal *et al*., Ischemic neurons prevent vascular regeneration of neural tissue by secreting semaphorin 3A. *Blood* **117**, 6024–6035 (2011).
51. K. Kucher *et al*., First-in-man intrathecal application of neurite growth-promoting anti-Nogo-A antibodies in acute spinal cord injury. *Neurorehabil. Neural Repair* **32**, 578–589 (2018).
52. V. Labat-gest, S. Tomasi, Photothrombotic ischemia: A minimally invasive and reproducible photochemical cortical lesion model for mouse stroke studies. *J. Vis. Exp.*, e50370 (2013).
53. R. Rust, L. Grönnert, B. Dogançay, M. E. Schwab, A revised view on growth and remodeling in the retinal vasculature. *Sci. Rep.* **9**, 3263 (2019).
54. J. R. Weis, B. Sun, G. M. Rodgers, Improved method of human umbilical arterial endothelial cell culture. *Thromb. Res.* **61**, 171–173 (1991).
55. M. V. Tsurkan *et al*., Defined polymer-peptide conjugates to form cell-instructive starPEG-heparin matrices in situ. *Adv. Mater.* **25**, 2606–2610 (2013).